Contributions of Individual Atmospheric Diabatic Heating Processes to the Generation of Available Potential Energy

JOY ROMANSKI

Center for Climate Systems Research, Columbia University, New York, New York

WILLIAM B. ROSSOW

City College of New York, City University of New York, New York, New York

(Manuscript received 23 July 2012, in final form 11 December 2012)

ABSTRACT

The generation of zonal and eddy available potential energy (G_z and G_e) as formulated by Lorenz are computed on a global-, daily-, and synoptic-scale basis to consider the contribution of each diabatic heating component separately and in combination. Using global, mostly satellite-derived datasets for the diabatic heating components and the temperature enables us to obtain G_z and, especially, G_e from observations for the first time and at higher temporal and spatial resolution than previously possible. The role of clouds in maintaining G is investigated.

The global annual mean G_z is 1.52 W m^{-2}. Values reach a minimum of 0.63 W m^{-2} in the Northern Hemisphere during spring and a maximum of 2.27 W m^{-2} in the Southern Hemisphere during winter. The largest contributors to G_z are latent heating in the tropical upper troposphere, associated with the intertropical convergence zone in the summer hemisphere and surface sensible heat fluxes in the winter pole. Diabatic cooling by radiative fluxes (mostly longwave) generally destroys G_z.

The value of G_e is negative and is about an order of magnitude smaller than G_z, with a global annual mean of -0.29 W m^{-2}. However, the small value of G_e results from the cancellation of the contributions from the individual diabatic heating terms, which are actually roughly similar in magnitude to their G_z contributions.

The results presented herein suggest that the large-scale dynamics of the atmosphere organize the spatial and temporal distribution of clouds and precipitation in such a way as to increase the energy available to drive the circulation, a kind of positive feedback.

1. Introduction

The circulation of the atmosphere is driven by and tries to eliminate the equator-to-pole temperature gradient, which is forced by latitudinally varying insolation. Exactly how this takes place is the result of complex interactions among the various components of the climate system.

One way to look at these interactions is via the Lorenz energy cycle, which is a compact way to summarize the flow of energy within the atmospheric general circulation; from generation, by diabatic heating of available potential energy (A, defined as that part of the potential energy in excess of the potential energy in a horizontally uniform, stably stratified, minimum potential energy reference state), conversion of A to kinetic energy (K) by fluid dynamical processes, and finally, dissipation of K by momentum mixing and friction processes (Lorenz 1955). Kinetic energy, available potential energy, and the conversion terms depend on the three-dimensional distributions of winds, geopotential, and temperature, and so they may be and have been computed from conventional weather observations (radiosondes), as done most notably by Oort and colleagues [see Peixoto and Oort (1992) for references]; however, frictional dissipation and generation of A depend on quantities that are not often measured and so were computed in previous analyses as residuals assuming energy equilibrium (Clapp 1961; Brown 1964; Siegmund 1994). The key uncertainty of the residual calculations comes from determining the vertical motions of the atmosphere, especially for eddies,

Corresponding author address: Joy Romanski, Center for Climate Systems Research, Columbia University, 2880 Broadway, New York, NY 10025.
E-mail: jr988@columbia.edu

DOI: 10.1175/JCLI-D-12-00457.1

because they are not measured by radiosondes. The errors are exacerbated by the incomplete global coverage of the radiosonde network, which is especially lacking in polar regions and the Southern Hemisphere. The generation of A_z (G_z) is expected to be positive as it is the basic input of energy into the system, but early studies of the generation of A in midlatitudes reached conflicting conclusions regarding the sign of the generation of A_e (G_e) (Suomi and Shen 1963; Hansen and Nagle 1984). Neither the sign nor magnitude of G_e is well determined because of insufficient space–time resolution of the conventional weather observations [Oort and Peixoto (1983), for instance, use monthly mean quantities]. Thus, G is not well quantified. Moreover, the residual calculation does not allow one to determine the separate contributions to G by the different diabatic heating processes, so these contributions have not been quantified before.

The approximate forms of G_z and G_e depend on the correlation between the deviation from the average temperature on an isobaric surface and the deviation from the average diabatic heating, which is composed of the radiative flux convergence, the net latent heating by precipitating cloud systems, and the surface sensible heat flux (Lorenz 1955). In other words, A is created when warmer regions are heated or colder regions are cooled and destroyed when warmer regions are cooled or colder regions are warmed. With the advent of global, satellite-derived products, it has become possible to compute the diabatic heating directly from observations and in much more detail. In particular, we can now quantify the individual contributions that each process makes to G, as well as using finer time resolution results to estimate G_e.

Recent estimates of G_z and G_e have been made from reanalysis datasets (Li et al. 2007; Boer and Lambert 2008); however, they were also computed from residuals in the energy cycle. These estimates still suffer from a lack of observational constraint on vertical velocity. Other studies have estimated G using diabatic heating inferred from the forced response of a weather forecast model (Haimberger and Hantel 2000; Steinheimer et al. 2008), which depends directly on model parameterizations of clouds, precipitation, and radiative processes. Those estimates of G are larger than the value presented here, varying from 2.1 W m^{-2} [total G from the National Centers for Environmental Prediction–National Center for Atmospheric Research (NCEP–NCAR) reanalysis for the years 1979–95] at the low end (Boer and Lambert 2008) to 3.0 $\pm$ 0.2 W m^{-2} (G_{grid}, the version of G comparable to the classical Lorenz formulation, which neglects subgrid-scale contributions) at the upper end (Steinheimer et al. 2008). Both used monthly means for their respective contributions, so their results are most comparable to our G computed using monthly mean input data, with vertical profile information -1.57 W m^{-2} (Romanski 2009). It is probable that some of the difference between our estimate and theirs (as well as the differences among their estimates) is due to the different time periods analyzed and different data sources, but it is also possible that our estimate is systematically smaller than the others for physical reasons. As noted by Haimberger and Hantel (2000), frictional dissipation is a source of heat for the atmosphere, although it is smaller than the other three components of the diabatic heating. Traditionally, this process has been considered part of the internal energy and not regarded as a contributor to G. It does, however, vary spatially in accordance with the prevailing winds, surface characteristics, and wind shear and could, when correlated with temperature, contribute to G. We also neglect the effect of vertical advection of sensible heat by convective motions. Transferring sensible heating from the lower troposphere to the middle troposphere would reduce its effect on G by moving heating to a region of smaller temperature contrasts, so neglecting this contribution may increase G by a small amount. Another possible source of G not accounted for in this study is the interaction between landscape variability and mesoscale flow, as described by Baldi et al. (2008); however, the magnitude of this possible source of G is not provided.

We used the longest period of overlapping data available at the time of the study; however, the short record may have biased our results and contributed to the discrepancies between our estimates and those of earlier studies. Marques et al. (2009) computed G_z and G_e from NCEP–NCAR for 1979–2001 and 40-yr European Centre for Medium-Range Weather Forecasts (ECMWF) Re-Analysis (ERA-40) for 1958–2001. They find that 1997–2000 had somewhat larger values of G_z and G_e than the 1979–96 period, but that comparably large values of both G_z and G_e were common in the ERA-40 record prior to 1979. Because of the different computation method and different data sources, it is not necessarily a given that we would have found the same long-term variability had we had a longer record available, but their findings suggest that it is possible that we sampled 4 yr with somewhat larger G_z and G_e than usual.

Our estimates of G are the only ones that are computed from diabatic heating calculated directly from observations and the only ones that decompose G_z and G_e into the contributions from each separate heating process, thus permitting evaluation of the role of cloud processes. Since we calculate diabatic heating from observations, we can link the various contributions to the physical processes that generate them and to the

atmospheric circulation, so that we can diagnose, in a physically meaningful way, how the atmosphere's circulation modifies the spatial distribution of heating away from the simple pattern of net solar radiation.

2. Analysis method

Only a portion of the total potential (internal plus potential) energy is available for conversion to kinetic energy, while the rest is used to maintain the vertical structure of the atmosphere against gravity. That energy that may be converted to kinetic energy is referred to as the available potential energy (A) and is defined as the difference between the actual total potential energy of the atmosphere and a theoretical reference state of minimum total potential energy that could result from any adiabatic redistribution of mass, that is, a statically stable barotropic atmosphere (Lorenz 1955, 1967). Any deviation from horizontal density stratification creates a horizontal pressure gradient, which may drive conversion from potential energy to kinetic energy. Although the dynamical wave regime in the tropics differs from the baroclinic wave regime at higher latitudes, the coupling of large-scale waves and deep convection that plays a role in phenomena like the Madden–Julian oscillation and the African easterly waves and may be responsible for the formation of mesoscale-organized convective systems warrants an evaluation of the ''eddy'' component of the generation of A by the diabatic heating processes. The approximate expression given by Lorenz (1955) for A as a function of the variance of temperature on isobaric surfaces is used herein, and A is decomposed into its zonal and eddy components, A_z and A_e. Balance equations for A_z and A_e and the zonal and eddy kinetic energies K_z and K_e are formed from their time derivatives. The source terms for A_z and A_e are given by the generation G in watts per square meter:

$$G_z = \int \Gamma([T] - \tilde{T})([Q] - \tilde{Q})\, dm = \int \Gamma[T'Q']\, dm, \quad (1)$$

$$G_e = \int \Gamma[T^*Q^*]\, dm, \quad (2)$$

where T is temperature, Q is the total diabatic heating (the sum of the individual diabatic heating components Q_{LH}, Q_{rad}, and Q_{sfc}), $\Gamma = (\gamma d/\tilde{T})(\gamma d - \tilde{\gamma})^{-1}$ is the stability parameter, γ is the lapse rate, γ_d is the dry adiabatic lapse rate, dm is a mass element, square brackets denote the zonal mean, prime denotes the departure from the global mean, asterisk denotes the departure from the zonal mean, and tilde denotes the global mean over an isobaric surface. Values of G presented herein refer to the contribution from a unit area (or average unit area); to find the contribution over a region, it is necessary to multiply by the area of that region (e.g., 2.56×10^{14} m^2 for a hemisphere or 5.12×10^{14} m^2 for the globe).

The value of G is computed separately for four vertical layers: the lower troposphere (surface to 680 mb), middle troposphere (680–440 mb), upper troposphere (440–100 mb), and above [100 mb to top of the atmosphere (TOA)]. We computed the anomaly of the layer mean temperatures from the global mean in the case of zonal available potential energy and from the zonal mean in the case of eddy available potential energy for each tropospheric and stratospheric layer, and then we computed the product of the temperature anomaly and the diabatic heating anomalies for each layer for both zonal and eddy quantities. These were integrated over space to yield the global and hemispheric generation of zonal and eddy available potential energy. The contribution to G_z and G_e by each component of the diabatic heating was computed separately (i.e., the integral over the atmosphere of $T'Q'$ or T^*Q^* for each individual component of the total Q) in order to compare it with the other terms and with the total.

3. Data

We use satellite-derived datasets wherever possible because they afford the most complete, uniform global coverage with the daily mesoscale sampling needed to resolve the synoptic weather observations, which is especially crucial to estimating G_e. Determinations of radiative fluxes, latent heating, surface sensible heat flux over oceans, and temperature are obtained from the International Satellite Cloud Climatology Project flux data (ISCCP-FD), the Global Precipitation Climatology Project (GPCP), and the Goddard Satellite-Based Surface Turbulent Fluxes (GSSTF) datasets. Surface sensible heat fluxes over land (except Antarctica) are obtained from the Global Land Data Assimilation System (GLDAS), which incorporates satellite data as well as other observations as forcings for its land surface modeling system, while surface fluxes over Antarctica are obtained from the NCEP–NCAR reanalysis, as there is no direct observation-based dataset available. The period 1997–2000 was chosen because it was the longest period of overlap between the various datasets at the beginning of this study. The analysis is performed at the highest temporal and spatial resolution possible given the characteristics of each dataset: daily, 2.5° longitude and latitude, with four atmospheric layers (surface to 680 mb, 680–440 mb, 440–100 mb, and 100 mb to TOA).

a. Radiative fluxes: ISCCP-FD

The ISCCP-FD provides global shortwave (0.4–5 μm) and longwave (5–200 μm) radiative fluxes at the surface, 680 mb, 440 mb, 100 mb, and the TOA every 3 h at 2.5° resolution for July 1983 through December 2009. It is created using the National Aeronautics and Space Administration (NASA) Goddard Institute for Space Studies (GISS) general circulation model (GCM) radiative transfer code and global datasets, cloud properties from ISCCP, temperature and humidity information from the Television and Infrared Observation Satellite (TIROS) Operational Vertical Sounder (TOVS), ozone information from the Total Ozone Mapping Spectrometer (TOMS), cloud vertical structure information from a climatology of rawinsonde humidity profiles (Rossow et al. 2005), stratospheric aerosol and water vapor data from the Stratospheric Aerosol and Gas Experiment II (SAGE-II), a seasonal cloud particle size climatology, an NCEP-1 reanalysis climatology of diurnal near-surface air temperature variations, tropospheric aerosols from the GISS GCM, and emissivity variations as a function of land cover type and the information on the spectral dependence of land surface albedo from the GISS GCM (see Zhang et al. 2004 for details and references). Uncertainties of monthly mesoscale fluxes are estimated to be in the range of 5–10 W m^{-2} at the TOA and 10–15 W m^{-2} at the surface, and daily mesoscale fluxes are estimated to be in the range of 10–15 W m^{-2} at the TOA and 20–25 W m^{-2} at the surface (Zhang et al. 2004). The estimated uncertainty in heating profiles is based on uncertainties in cloud vertical distribution, and while the estimated uncertainty in the magnitude of the cloud effect at any particular level is 25%–50% (Chen et al. 2000), the total optical thickness of the clouds in the column constrains the total uncertainty in heating rates to about 10%.

b. Precipitation: GPCP

Global daily estimates of precipitation at a resolution of 1° are obtained from the GPCP 1-degree daily (1DD) precipitation dataset (version 2). GPCP 1DD is produced using microwave radiances from polar-orbiting satellites and infrared (IR) brightness temperatures from geostationary satellites, merged with rain gauge data over land. Data are available from October 1996 to the present, delayed by a few months for processing. Validation experiments have been conducted in a variety of locations worldwide and suggest that, while there are known problems in regions of persistent convective precipitation, nonprecipitating cirrus, and complex terrain, the GPCP 1DD product performs as well as other rainfall datasets (Huffman et al. 2001). The estimated uncertainty of monthly regional mean precipitation rates is overall about 10%–15%, with a larger proportion of uncertainty in polar regions. The estimated uncertainty in daily precipitation rates is larger, as much as 25%–50% (see Huffman et al. 2001; Adler et al. 2003).

c. Surface sensible heat fluxes

1) OCEANS: GSSTF

The GSSTF, version 2 (GSSTF2), dataset is generated at the NASA Goddard Space Flight Center (GSFC) and provides surface turbulent fluxes over the global ocean using surface (10 m) winds from the Special Sensor Microwave Imager (SSM/I), precipitable water from SSM/I, sea surface temperature, 2-m air temperature, and sea level pressure from the NCEP–NCAR reanalysis as inputs to a bulk flux model. Daily data are available from July 1987 through December 2000 at 1° resolution [production of an improved version of this product has resumed (version GSSTF2b), and data are now available from July 1987 to December 2008]. Comparisons with fluxes measured in field experiments indicate that the daily surface sensible heat fluxes have an uncertainty of 10 W m^{-2} and a positive bias of 6 W m^{-2}, with an overall correlation of 0.84 (Chou et al. 2003). Chou et al. estimate monthly mean flux uncertainties of 10%–15%, but other studies indicate some larger uncertainties (Romanou et al. 2006). Daily mean flux uncertainties may be as large as 20–25 W m^{-2} (Curry et al. 1999, 2004).

2) LAND NORTH OF 60°S: GLDAS

The GLDAS dataset incorporates Advanced Very High Resolution Radiometer (AVHRR) measurements of vegetation, ground-based soil observations, digital land slope and elevation, TOVS skin temperature, the Air Force Weather Agency's snow cover data, surface forcing fields of precipitation, downwelling longwave and shortwave radiation, near-surface air temperature and near-surface specific humidity, near-surface u- and v- winds, and surface pressure from either data assimilation systems [the Goddard Earth Observing System (GEOS) Data Assimilation System, the Global Data Assimilation System (GDAS), or the ECMWF] or datasets derived from satellite-based observations of these quantities to both force and constrain land surface models in order to generate a dataset of land surface conditions and fluxes (see Rodell et al. 2004 for details and references). Validation is not yet complete (Rodell et al. 2004). This study used 3-h data at 0.5° resolution, but data are now available for 1979 through present at 1° and 0.25° resolution.

3) LAND SOUTH OF 60°S: NCEP–NCAR REANALYSIS

The NCEP–NCAR reanalysis uses a data assimilation system to incorporate a wide variety of observations into an atmospheric GCM. Thus, the output is a combination of measured values where they are available and modeled values based on the measurements. The reanalysis extends from 1948 to the present, with daily global coverage on a 192 × 92 Gaussian grid for the surface sensible heat flux (Kalnay et al. 1996). Large errors in energy divergence over Antarctica suggest that the sensible heat flux in that region may not be very accurate (Trenberth et al. 2001, 2002), so results obtained for this area will be treated as less certain.

d. Atmospheric temperature: TOVS

TOVS atmospheric temperature profiles are produced by the National Oceanic and Atmospheric Administration (NOAA) using information obtained from the three instruments that make up the TOVS system: the High Resolution Infrared Radiation Sounder (HIRS/2), the Stratospheric Sounding Unit (SSU), and the Microwave Sounding Unit (MSU) (Kidwell 1995). This study will use the ISCCP version of TOVS, which supplements the original TOVS temperature and humidity data with a global rawinsonde climatology to fill in missing data. Additionally, ISCCP vertically interpolates from the original TOVS pressure levels to those used in the ISCCP dataset (Rossow et al. 1996). The data are available for the period July 1983 through December 2009 every 3 h at 2.5° resolution. TOVS temperature measurements have uncertainties of 2–3 K (Zhang et al. 2006).

e. Dataset modifications

All of the datasets were put into a common format, 2.5° equal-area horizontal grid and vertical resolution (where applicable) at daily intervals. For this analysis, vertical profiles were averaged into four atmospheric layers: a lower troposphere layer from the surface to 680 mb, a midtroposphere layer from 680 to 440 mb, an upper-troposphere layer from 440 to 100 mb, and a layer extending upward to the TOA. Lapse rates are computed at the original, higher vertical resolution and then averaged to the four vertical layers.

Latent heating profiles at the resolution of the ISCCP-FD data (three tropospheric layers and one stratospheric layer) were generated from the GPCP precipitation data. Lacking globally complete vertical measurements of rain rate like those provided by the Tropical Rainfall Measuring Mission (TRMM) precipitation radar instrument or (in the future) by *CloudSat*, we apportioned latent heating corresponding to the surface rainfall amount to the appropriate layer according to ISCCP cloud amount and vertical location as reported in the ISCCP-FD dataset (Rossow et al. 2005). This approach ensures that the altitude of latent heating from precipitation is consistent with the altitude of radiative heating by clouds. Comparison with vertical heating profiles taken from the literature (e.g., Tao et al. 2001, 2006; Magagi and Barros 2004; Turpeinen et al. 1990; Pauley and Smith 1988) suggests that this approach is adequate, given the crudeness of our vertical resolution.

f. Sensitivity analyses

As can be seen from Eqs. (1) and (2), G_z and G_e depend on the covariance between the latitudinal or longitudinal anomalies of temperature and diabatic heating. Hence, the data errors most likely to produce serious errors in G_z and G_e are spatially structured biases, either in the horizontal or the vertical, because these can change the magnitude or even the sign of the covariances. Unless it is very large relative to the data, random error will reduce the magnitude of G_z and G_e, but not by very much. A uniform bias will affect the mean temperatures and heating terms, but not the variances, and so will not change G_z or G_e. Bearing this in mind, and considering the estimated accuracy of each dataset, we have constructed test datasets to explore the impact on the results of the sort of errors we believe are most likely to be present that seriously affect G_z and G_e. The test datasets are described briefly in the appendix. Detailed descriptions, as well as figures showing the original and test datasets, are presented in Romanski (2009). The results of our sensitivity studies are summarized in Table A1.

The results of our sensitivity studies suggest that, while the test scenarios exhibit larger biases than we believe to be present, it is possible that our G_z estimates are too large in Northern Hemisphere (NH) winter and too large by a lesser amount in the Southern Hemisphere (SH) in both winter and summer. The value of G_e is probably not negative enough, especially in the NH winter. If we assume all of the errors described in the appendix are present, although to a lesser extent than assumed in our sensitivity studies, and that their effects on G_z and G_e sum linearly (worst case), we find that, partially because of fortuitous cancellation of errors of opposite signs, we may have overestimated G_z by as much as 20% during SH summer, 25% during SH winter, and 35% during NH winter. We may have underestimated the magnitude of G_e (a negative value, i.e., our value is probably not negative enough) by as much as 25% during NH winter, 10% during SH winter, and by a lesser amount otherwise. While we tested the various scenarios individually and did not assess the possibility

that multiple errors could occur at once, we believe that the scenario most likely to involve correlated errors is the too-warm polar surface temperatures and corresponding error in radiative flux. The effect of the temperature error was sufficiently small that we felt it was reasonable to consider only the effect of the related radiative flux error; however, it is possible that we are underestimating the effect of correlated errors in temperature and heating. Despite the large magnitude of the estimated uncertainties, coherent spatial and temporal patterns of G_z and G_e suggest that our results provide previously unavailable information about these important quantities. Additionally, errors of this magnitude will not affect our conclusions as to the relative magnitudes of G_z and G_e.

An upper limit on random uncertainty is set by the standard deviations of the diabatic components and total G_z and G_e. The standard deviation in time of global mean G_z within an individual season during the study period is generally approximately 20%–25% of the mean value. Examination of a Hovmöller plot of G_z and animations of daily maps of G_e over the study period reveal coherent temporal variations that are not random, suggesting that the random uncertainties are smaller than the standard deviations.

It is important to note that the exact and approximate formulations of G are not precisely the same. This study, as well as most other studies in the literature, uses the approximate formulation employed by Lorenz (1955), because of the difficulty of obtaining observations on isentropes as opposed to pressure surfaces. However, as noted by Dutton and Johnson (1967) and Siegmund (1994), while the global annual mean approximate and exact versions of G may not differ much, there can be biases in the regional contributions. The two most important differences between the two versions are due to approximating the average pressure on an isentrope by the pressure of the isobaric surface for which the average potential temperature is equal to the potential temperature of the isentrope (Siegmund 1994, Approximation II) and approximating the vertical variation in average pressure on an isentrope by the vertical variation in average potential temperature on an isobaric surface (Siegmund 1994, approximation IV). There are two areas where the impact will be greatest: the extratropical lower troposphere and the tropical middle and upper troposphere.

In the extratropical lower troposphere, the sign of G may differ depending on the formulation used. The exact form multiplies the diabatic heating by an efficiency factor E, which is the local departure of the pressure on an isentrope from its global mean. In the situation where a cold continental air mass passes over warm ocean near the east coast of continents in the midlatitudes during the NH winter, the local pressure on a near-surface isentrope is larger than the global mean pressure on that isentrope because of the strong upward curvature of isentropes as one moves poleward, and there would be weak positive generation. The same situation would destroy G in the approximate formulation, as surface sensible heat flux from the ocean warms the cold air. We tested this idea by examining five cases during January 1997 where cold, average, or warm air masses were above the central Sea of Japan (results not shown). We chose that region because there are strong incursions of cold air from the Asian continent, but we could also have used the east coast of the United States. In each case, the sign of the pressure anomaly with respect to the global mean pressure on the 285-K surface is negative; the local pressure is lower than the global mean pressure, not higher. According to Siegmund (1994) and Dutton and Johnson (1967), the exact formula states that potential energy is created when heating occurs at pressures higher than the global mean on a particular isentrope and is destroyed when heating occurs at pressures lower than the global mean. Here heating occurs at lower pressure because the sharp gradient in pressure on the 285-K surface occurs equatorward of the heating. Under these conditions, the exact formulation predicts negative generation, which agrees with our findings using the approximate formulation. This is a qualitative analysis of only a few cases, but it suggests that, at least some of the time, the exact and approximate formulations agree, rather than differ, on the sign of G_e in the case of cold air moving over warm oceans in midlatitude NH winter.

The approximate formulation uses a constant global mean static stability to scale the covariance of temperature and diabatic heating. Dutton and Johnson (1967) showed that using global mean rather than horizontally varying static stability results in overestimating the tropical contribution to A_z by up to 50% for the standard atmosphere lapse rate and by up to 30% using a time-varying, pressure-dependent lapse rate for a rather minimal sample of the atmosphere, a cross section along 75°W for 1958. Estimates of G are subject to similar biases, since the same expression for the static stability is used. We used time-varying, pressure-dependent lapse rates, so our bias would be closer to 30%, rather than 50%.

To assess the effect of using globally constant static stability, we tested the effect of zonally varying lapse rates and temperature on the stability parameter and then qualitatively estimated what impact that would have on the contributions from each diabatic heating term at each level (lower, middle, and upper troposphere) to our values of G_z (not shown). In each case, we used daily values, derived from TOVS temperatures.

TABLE 1. Estimates of the generation of available potential energy (W m^{-2}) for the NH, SH, and global atmosphere [after Peixoto and Oort (1992)] from this study and from Peixoto and Oort (P&O) and global annual means from Lorenz (1955). As in Peixoto and Oort, to obtain the integrals over the total atmospheric mass, multiply the values for the NH and SH by 2.56×10^{14} m^2 and the values for the globe by 5.12×10^{14} m^2. The abbreviations LH, Rad, and Sfc refer to the contributions to the generation of available potential energy due to latent heating, radiative flux convergence, and surface sensible heat flux, respectively.

			Year			DJF			MAM			JJA			SON		
			NH	SH	Globe	NH	SH	Globe	NH	SH	Globe	NH	SH	Globe	NH	SH	Globe
G_z	This study	LH	0.58	0.26	0.42	0.11	0.92	0.52	0.52	0.38	0.45	0.74	−0.26	0.24	0.97	0.01	0.49
		Rad	−0.17	−0.35	−0.26	0.02	−0.71	−0.34	−0.68	−0.02	−0.35	−0.05	0.03	−0.01	0.08	−0.74	−0.33
		Sfc	0.95	1.46	1.21	1.34	0.77	1.06	0.78	1.46	1.12	0.51	1.71	1.11	1.09	1.54	1.31
		All	1.38	1.65	1.52	1.51	1.03	1.27	0.63	2.17	1.40	1.29	2.27	1.78	2.17	1.06	1.61
	P&O		1.26	0.97	1.12	0.76	2.33	1.54				2.03	0.16	1.10			
	Lorenz				3.1												
G_e	This study	LH	0.21	0.09	0.15	0.51	0.09	0.30	0.13	0.12	0.12	−0.02	0.07	0.03	0.22	0.06	0.14
		Rad	−0.43	−0.26	−0.35	−0.56	−0.21	−0.38	−0.44	−0.30	−0.37	−0.30	−0.28	−0.29	−0.43	−0.23	−0.33
		Sfc	−0.07	−0.10	−0.09	−0.17	−0.07	−0.12	−0.08	−0.10	−0.09	0.10	−0.12	−0.01	−0.14	−0.09	−0.12
		All	−0.30	−0.27	−0.29	−0.21	−0.19	−0.20	−0.38	−0.29	−0.34	−0.21	−0.32	−0.27	−0.34	−0.26	−0.30
	P&O		0.7	0.7	0.7	0.5	0.7	0.6				1.0	0.4	0.7			

We performed the same computations with NCEP-2 temperatures and obtained substantially similar results (not shown). We also computed the stability parameter using gridded lapse rates and temperature, but it is more difficult to assess the impact on G_e because of the time-varying nature of the interactions between stationary features such as land–sea contrast and moving features such as midlatitude cyclones and anticyclones. Siegmund (1994) discusses the effect on global annual mean G using Lorenz's stability parameter and a zonally varying version used by Arpe et al. (1986) and finds that they are similar in the mean, but that Lorenz's version is better for most individual months.

We found that overall, biases cancel in the global mean, but the contributions from the lower and middle troposphere may be too large and the contribution from the upper troposphere too low. In general, using global mean temperature and lapse rate for static stability rather than zonally averaged temperature and lapse rates causes us to overestimate the contribution to G_z of polar winter surface sensible heat fluxes and to underestimate the contribution to G_z of latent and radiative heating in the tropical upper troposphere. This result is consistent with Siegmund's (1994) report that biases related to the use of the approximate formula cancel in the global mean, but it is not consistent with Dutton and Johnson's (1967) statement that a horizontally varying lapse rate would result in a better correspondence between the exact and approximate versions, especially in the tropical middle and upper troposphere. In fact, we find that the contributions to G_z in the tropical middle and upper troposphere obtained using global mean temperature and lapse rate to compute the stability parameter are smaller than those obtained using zonally varying temperature and lapse rate and, hence, are closer to the exact version.

4. Results

The annual and seasonal means of G_z for the globe, NH, and SH are presented in Table 1. The value of G_z is greater in the winter hemisphere than in the summer hemisphere, particularly in the SH. The global and hemispheric values of G_z and their seasonal variation reported herein differ from those shown in Peixoto and Oort (1992) (Table 1), who estimated a smaller global annual mean value of G_z and much larger seasonal hemispheric variations, with maximum values in the summer hemisphere. The global annual mean G_z is 1.52 W m^{-2}, considerably less than Lorenz's (1955) estimate of 3.1 W m^{-2}. Surface sensible heat flux is the largest contributor to G_z, except in the summer hemisphere, where it contributes slightly less than latent heating. Contributions from surface sensible heat fluxes peak in the winter hemisphere because large heat losses from the atmosphere to the surface at high latitudes create a strong latitudinal gradient in surface sensible heat flux. This pattern exists in both hemispheres and is stronger in the SH. Despite being roughly an order of magnitude smaller than latent and radiative heating, surface sensible heat fluxes have a large impact on G_z because they occur in the lower troposphere, where temperature gradients are largest and are better correlated with temperature anomalies.

Latent heating is a large contributor in the summer hemisphere tropics and winter hemisphere high latitudes, though still smaller than wintertime high latitude surface sensible heat fluxes. The net latent heating by precipitating cloud systems is the main source of heat to

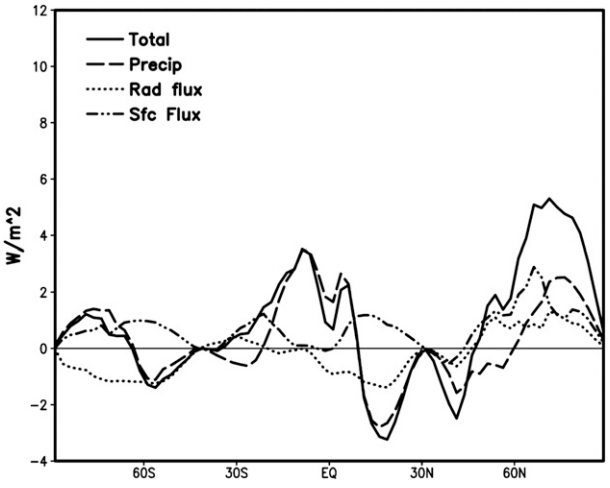

FIG. 1. The DJF mean individual diabatic heating contributions to zonal mean G_z. Values are computed from daily mean temperature and diabatic heating and have been weighted by the cosine of latitude.

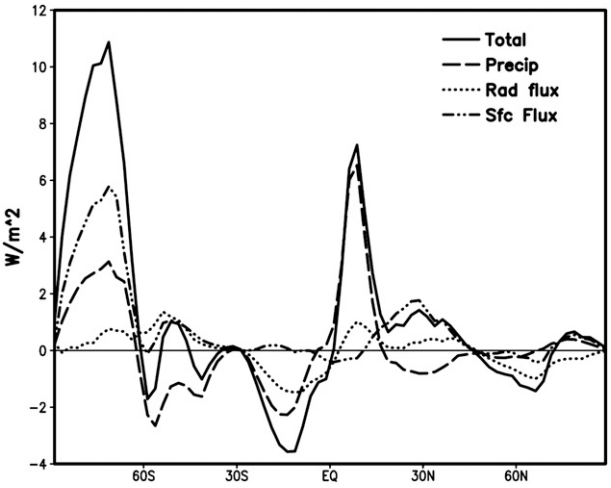

FIG. 2. As in Fig. 1, but for JJA.

the atmosphere, balancing radiative cooling. The energy balance of the surface is governed by evaporative cooling and solar heating. Since most clouds do not produce precipitation (Liu et al. 2008; Lin and Rossow 1997), their water content is returned to vapor within minutes to hours and with little shift in location (except possibly for some cirrus); hence, the atmospheric heating by precipitation is not necessarily collocated with the surface evaporative cooling. The formation of precipitation is controlled by horizontally convergent atmospheric motions (large-scale updrafts) or dynamic instabilities (convection) that depend on temperature gradients; thus, latent heating is less well correlated with temperature, reducing its effectiveness in generating A (e.g., Pauley and Smith 1988; Fuelberg et al. 1985; Robertson and Smith 1983; Hayashi and Golder 1981; Smith 1980).

The net radiative flux divergence in the atmosphere is dominated by longwave (thermal infrared) flux divergence as the atmosphere absorbs only about one-third of the total absorbed insolation (the rest heats the surface). In general, the radiation is a negative contribution to G because it tends to cool warmer locations more; however, clouds introduce some subtle changes by shifting weak solar heating upward and the dominant longwave cooling downward in the atmosphere (Zhang et al. 2004), thus acting to reinforce G_z (cf. Rossow and Zhang 1995). The contribution to G_z from radiative flux convergence is weakly positive in the winter hemisphere and strongly negative in the SH summer, but only weakly negative in the NH summer.

Figures 1 and 2, which show the zonal mean contributions of each diabatic heating term to the December–February (DJF) and June–August (JJA) mean G_z, respectively, reveal that in both seasons, the winter pole is a strong contributor to G_z, with all three diabatic heating components working together there. The tropics feature strong positive contributions in the summer hemisphere from latent heating, especially in the NH. The zonal mean contributions to G_z from each diabatic heating component during the transition seasons resemble that of the annual mean values (not shown).

Table 1 also presents the annual and seasonal mean G_e for the globe, NH, and SH. The value of G_e is negative and about an order of magnitude smaller than G_z. While these values do not match any prior estimates of G_e, they confirm Lorenz's supposition that G_e would be negative (Lorenz 1955). Note that prior estimates were based on monthly averaged data, whereas ours are based on daily data; this has been shown to change computed values of G_e from negative to near zero or slightly positive (Romanski 2009). Although G_e is much smaller than G_z, Table 1 shows that this results from cancellation of opposing contributions from latent heating and radiative fluxes that are roughly the same order of magnitude as their contributions to G_z, combined with much smaller contributions from surface sensible heat fluxes. In the hemispheric mean, negative contributions to G_e from radiative fluxes and surface sensible heat fluxes combine to overpower positive contributions from latent heating, although this is not necessarily true regionally or in the zonal mean. This is in contrast to G_z, where the surface sensible heat fluxes reinforce latent heating. The quantity G_e attains its largest negative values during the transition seasons because the positive contribution from latent heating is lower and cannot overcome the negative contributions from radiative and surface sensible heat fluxes (not shown). The one exception is in the NH summer, where latent heating is a negative

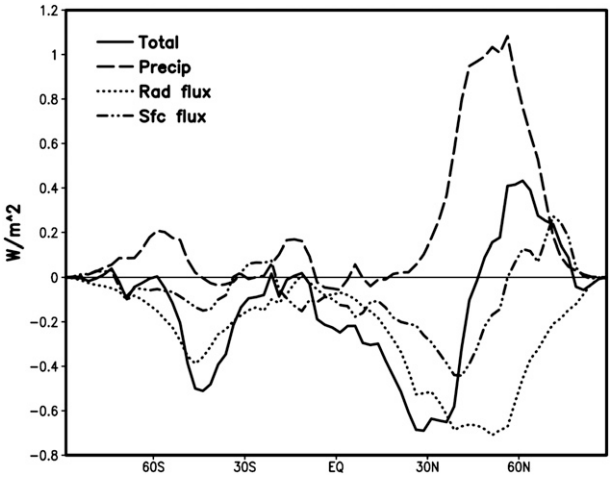

FIG. 3. As in Fig. 1, but for G_e.

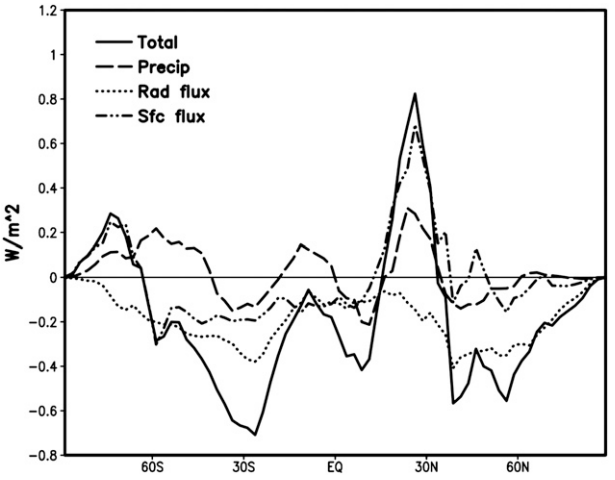

FIG. 4. As in Fig. 3, but for JJA.

contributor and surface sensible heat fluxes are a positive contributor.

Figures 3 and 4 show the contributions of each diabatic heating component to the zonal mean G_e for DJF and JJA, respectively. The SH behaves largely the same in both summer and winter, with a few small differences. Summer and winter are both characterized by a large positive contribution from latent heating in the subpolar region and negative radiative flux contributions. In DJF, the minimum contributions from radiative flux shift poleward from the subtropics to the midlatitudes. Surface sensible heat fluxes are a positive contribution in high latitudes during both seasons, but especially during winter. The SH March–May (MAM) and September–November (SON) contributions to G_e are broadly similar to each other (not shown) and to the annual mean.

The NH is very different from winter to summer. In winter, the contribution from latent heating shifts from a narrow peak in the subtropics poleward to a broad peak encompassing all of the midlatitudes, and it is much larger in magnitude than in summer. However, it is opposed in the midlatitudes by contributions by surface sensible heat fluxes and radiative fluxes, which are strongly negative over most of the Northern Hemisphere. In the subpolar region, surface sensible heat flux contributions become positive and act with latent heating to counter the negative contribution of radiative fluxes. In summer, strong surface fluxes combine with latent heating in the subtropics to produce a large positive G_e despite a negative contribution from radiation. In the mid and high latitudes during JJA, contributions to G_e from surface sensible heat fluxes and latent heating are near zero, and G_e is dominated by the negative contribution from radiative fluxes. As in the SH, the MAM and SON contributions of the individual diabatic heating components to the zonal mean G_e resemble each other and the annual mean (not shown).

Figure 5, maps of the DJF mean total column G_e, and individual diabatic heating contributions, reveal that the small negative values of G_e seen in the global and hemispheric means are the sum of regions of strong positive and negative G_e. Radiative flux convergence is always a negative or neutral contributor. Latent heating is nearly always a positive or neutral contributor and is especially pronounced over the NH midlatitude storm tracks and the eastern sides of Asia and North America. Surface sensible heat fluxes contribute both positively and negatively to G_e. The distribution of G_e during DJF is a result of the competition between radiative cooling and latent heating, with surface sensible heat fluxes acting to reinforce the resulting pattern.

In JJA, the areas of maximum positive G_e in the NH midlatitude ocean basins shift equatorward from their positions in DJF (Fig. 6). SH JJA patterns lack the storm track and continental areas of positives and negatives seen in the NH during DJF; instead, land areas and oceans are mostly negative and Antarctica is a positive contributor to G_e. In general, in the NH, radiation and latent heating are strong in different regions and so do not compete as in DJF. The spatial distribution of contributions to G_e during MAM is similar to JJA, but with weaker positive contributions. The map of G_e contributions during SON resembles that during DJF, but with weaker positive regions (not shown). In both transition seasons, the negative contributions to G_e are of similar strength and spatial structure as the following extreme season: MAM is similar to JJA, and SON is similar to DJF.

Daily and 30-day running averages of time series of global mean G_z and G_e are shown in Figs. 7 and 8,

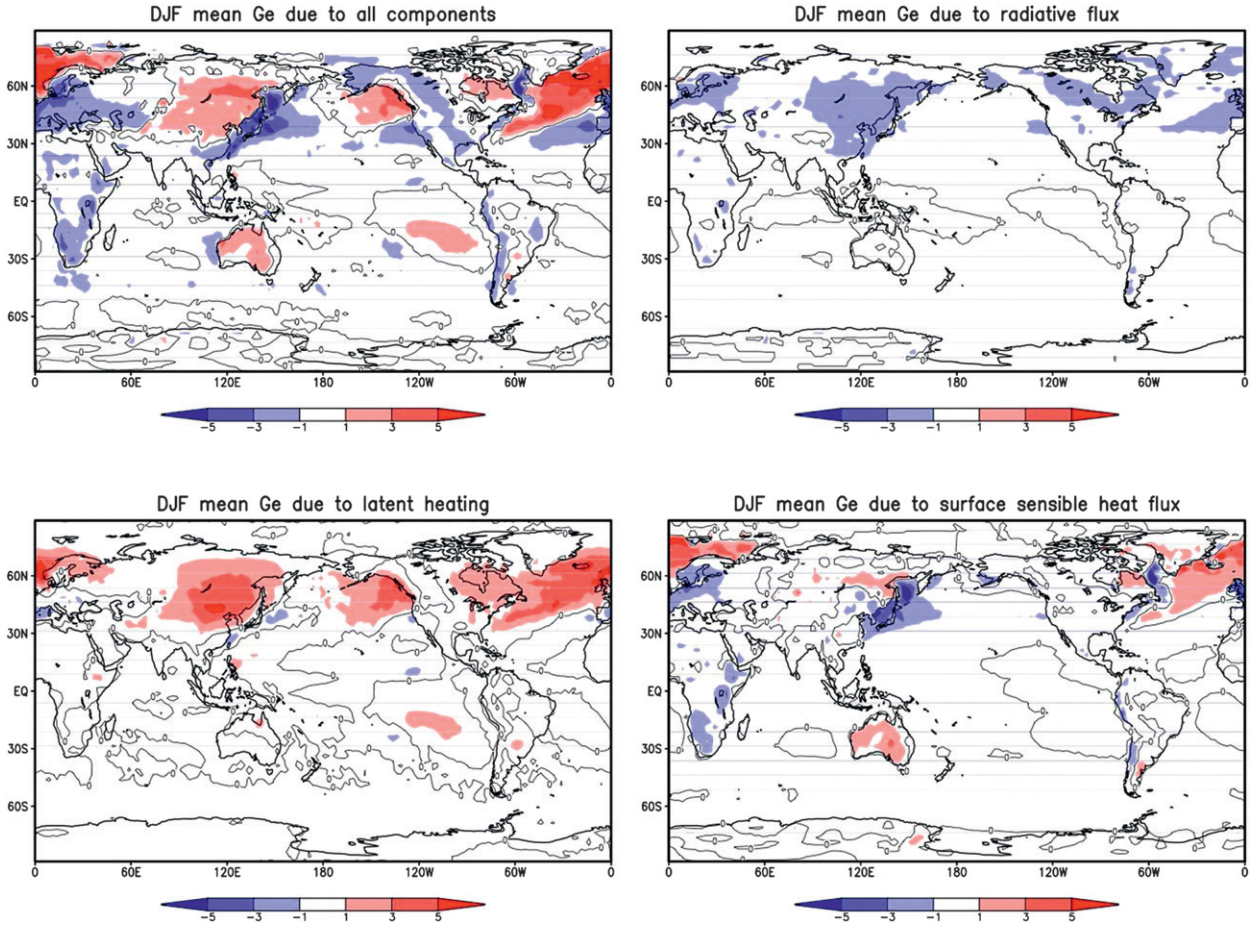

FIG. 5. The DJF mean total column G_e and G_e due to all and individual diabatic heating, components (W m^{-2}).

respectively. Short period variability (i.e., submonthly) is present in both but contributes a greater portion of the overall variability of G_e than G_z. The quantity G_z appears to contain a downward secular trend over the study period, but the brevity of the available data record does not permit us to draw any conclusions regarding it; G_e does not display this apparent trend. The quantity G_z varies semiannually, with a strong peak in July/August and a weaker peak in February/March; G_e also varies semiannually, with peaks of equal amplitude occurring in June and December.

Figures 9 and 10 show 30-day running means of the total and individual contributions to G_z from each diabatic heating component in the NH and SH. Both hemispheres show similar short period variability to that seen in Fig. 9, with latent heating having the largest amplitude at that time scale, but for clarity only the 30-day running means are shown. Figures 9 and 10 make it clear that the apparent weak semiannual variation of G_z visible in Fig. 7 results from the sum of opposite-phase annual cycles in the NH and SH, with the stronger annual cycle in the SH. The value of G_z in both hemispheres peaks in that hemisphere's winter, although the peak occurs later in the winter in the SH than in the NH, which peaks in late fall–early winter. The amplitude and phase of the NH annual cycle of G_z agrees with an earlier estimate by Oort and Peixoto (1976), but they found somewhat larger interannual variability in both the maxima and minima. In both hemispheres, surface sensible heat fluxes are the largest contributor to G_z except during summer, when latent heating is the largest. The magnitude of the surface flux contribution is substantially larger in the SH than in the NH, accounting for most of the difference in the amplitude of the annual cycles in the two hemispheres. Latent heating also has a larger annual cycle and a larger peak positive contribution in the SH than in the NH, whereas radiative fluxes have a similar magnitude in both hemispheres. SH latent heating is out of phase with both radiative and surface fluxes, whereas in the NH, they are only slightly out of phase. In the SH, latent heating peaks sharply in summer and has a broad minimum in winter. The NH

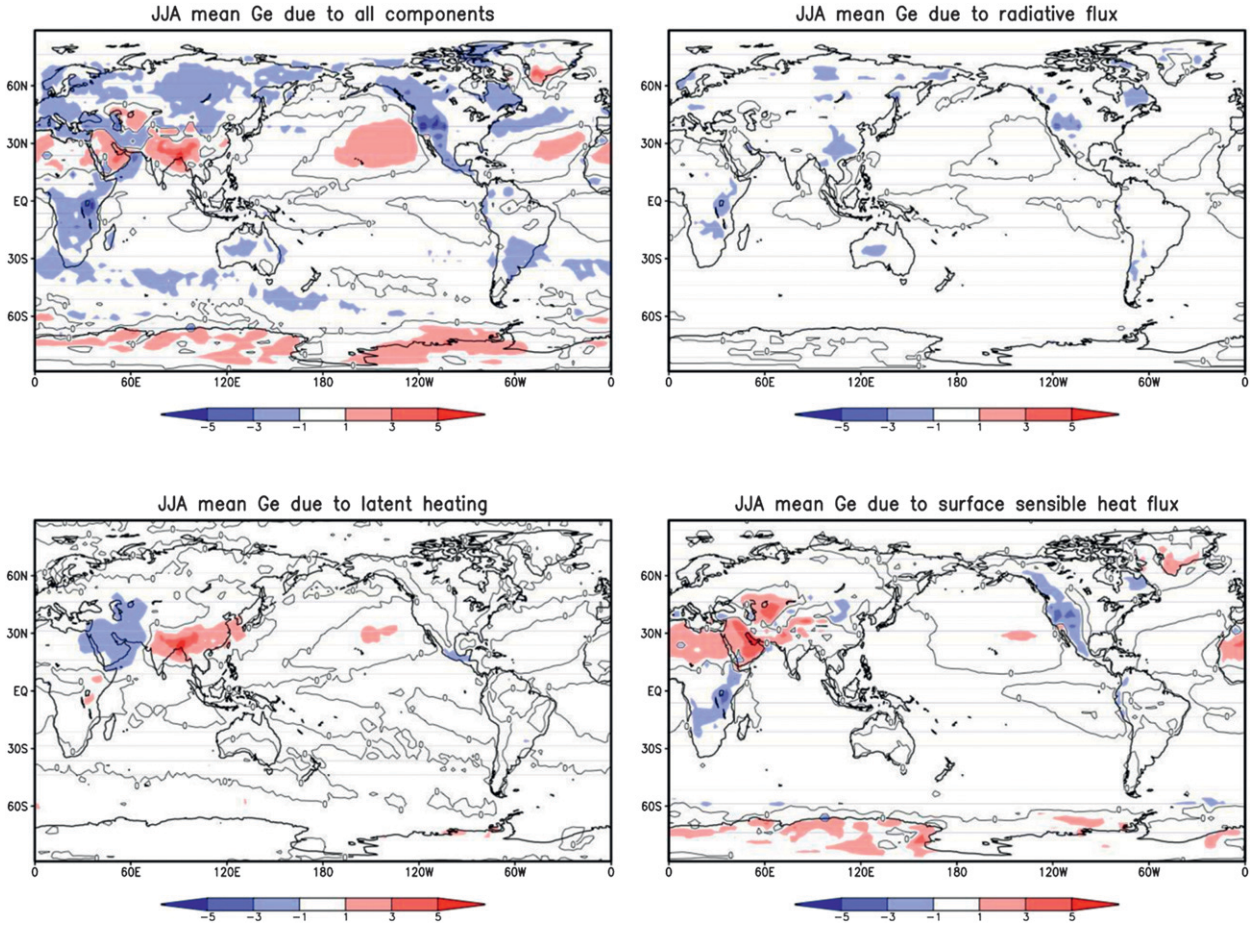

FIG. 6. As in Fig. 5, but for JJA.

pattern is reversed, with a broad summertime peak, sometimes with a local midsummer minimum and a sharp winter minimum. This may be because of the mean position of the ITCZ in the NH; the maximum of tropical convection spends more time in the NH than the SH.

Figures 11 and 12 show 30-day running means of the total and individual component time series of G_e; G_e has a semiannual cycle in the NH and no obvious seasonal cycle in the SH. The NH has maxima in winter and summer and minima in the transition seasons. Latent heating is the main contributor with peaks in winter. Surface fluxes and radiation are in phase, reaching maxima in summer and minima in winter. The semiannual cycle results from the combination of the individual components.

The time series of individual diabatic heating component contributions to G_e in the NH (Fig. 9) shows that the contribution from latent heating is smaller than usual in the NH during the historical El Niño in DJF 1997/98. Both the gradients of temperature and latent heating contribute to G_z. Comparison of zonal mean latent heating from precipitation and zonal mean temperature for DJF 1997/98 with those for all four winters (not shown) reveals a small warming signal throughout the tropics, in agreement with Trenberth and Smith (2006), but the increase in the gradient is small compared to the magnitude of the

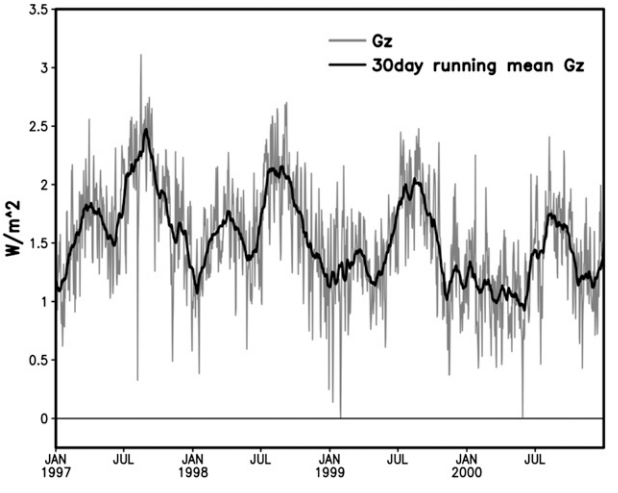

FIG. 7. Daily and 30-day running mean global mean G_z.

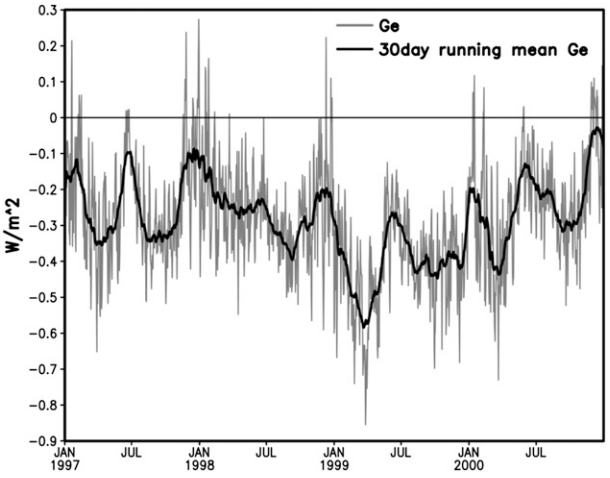

FIG. 8. As in Fig. 7, but for G_e.

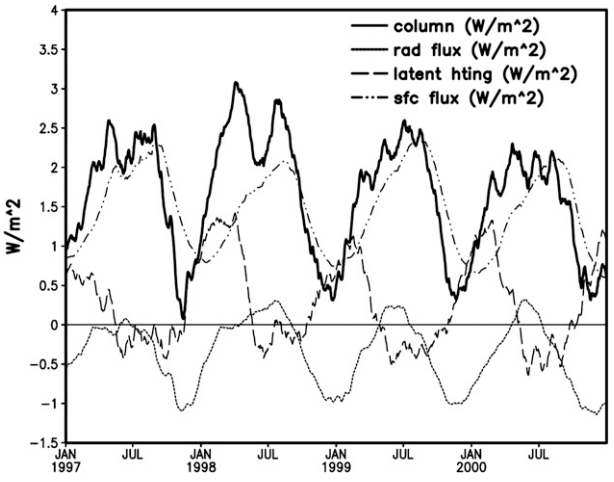

FIG. 10. As in Fig. 9, but for the SH.

gradient itself. However, the ENSO-induced precipitation shifts (described by, e.g., Curtis et al. 2001) produced a shift in the latitude of zonal mean latent heating from the NH deep tropics to the equator and just south of the equator, as well as an increase in latent heating in the NH subtropics. Reducing the latent heating in the NH deep tropics decreased the magnitude of the NH latitudinal gradient of latent heating, suppressing G_z production there.

Figure 11 shows enhanced G_e production by latent heating during DJF 1997/98. Examination of G_e production by latent heating during that winter (not shown) reveals intensification of the usual pattern of G_e production in the NH midlatitude storm tracks. There was no effect on tropical G_e because of the small tropical temperature gradients, even in an intense El Niño.

5. Discussion

Our estimates of G_z are in between Lorenz's (1955) estimate of 3.1 W m^{-2} for the global annual mean and the estimates computed by Peixoto and Oort (1992) using radiosonde data (Table 1), though closer to Peixoto and Oort's values. Peixoto and Oort found a global annual mean G_z of 1.12 W m^{-2}, maximum G_z of 2.33 W m^{-2} during DJF in the SH, and minimum G_z of 0.16 W m^{-2} during JJA in the SH. We find a smaller amplitude seasonal cycle in each hemisphere than Peixoto and Oort, smaller contrast between the hemispheres during each season than Peixoto and Oort, and maximum G_z in the winter hemisphere, unlike Peixoto and Oort, who found maximum G_z in the summer hemisphere. We believe that a key reason for this discrepancy is the incomplete global coverage of the radiosonde data, which are concentrated in the midlatitude

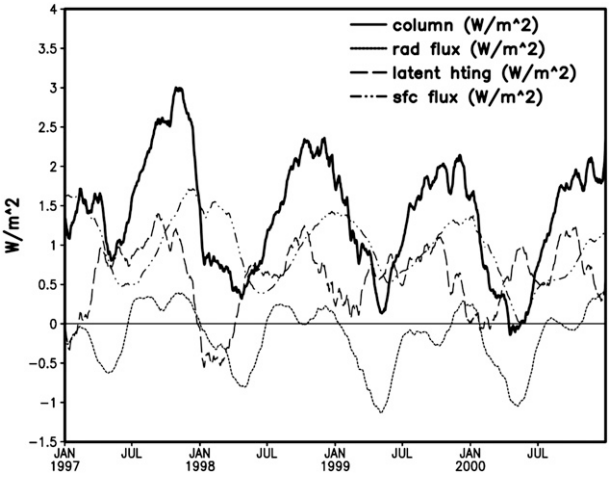

FIG. 9. The 30-day running mean of individual diabatic heating contributions to the NH, mean G_z.

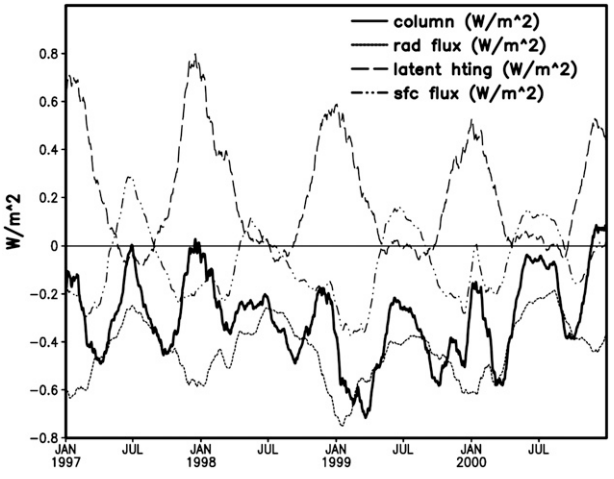

FIG. 11. As in Fig. 9, but for G_e.

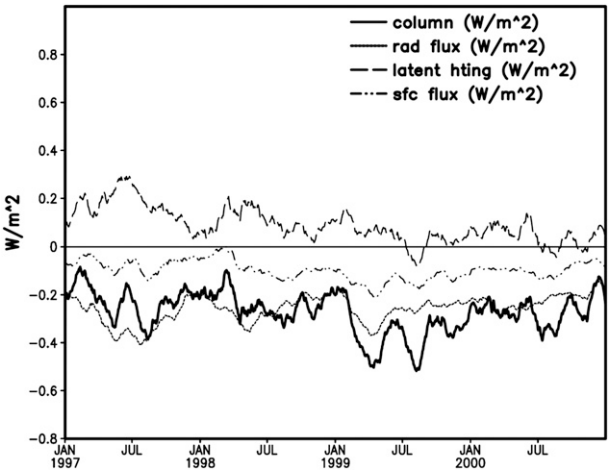

FIG. 12. As in Fig. 11, but for the SH.

land areas of the NH. Considering that G_z is sensitive to the latitudinal gradients of temperature and diabatic heating, it seems plausible that a paucity of data in the polar regions would contribute to an underestimate of wintertime G_z, when cold polar temperatures lead to a large latitudinal gradient in temperature and surface sensible heat flux and also to an overestimate of summertime G_z when the latitudinal gradients of temperature and surface sensible heat flux are less correlated. While we did not conduct a sensitivity study designed to replicate this particular scenario, we can infer from the results of our other sensitivity tests (especially 1b and 1c, see Table A1), in which we altered the latitudinal gradient of heating, that undersampling the latitudinal gradient of diabatic heating could have a very large effect on G_z, possibly enough to change the season of maximum G_z. The difference between our findings and Peixoto and Oort's is especially striking in the case of the SH during JJA; we find this is the largest seasonal hemispheric contribution to G_z, while Peixoto and Oort found it to be the smallest. Lack of data in most of the SH, especially during winter, could cause such a large discrepancy.

Our finding that the global and hemispheric mean G_e is generally negative is in contrast to Peixoto and Oort's (1992) estimated values of G_e, which ranged between 0.4 and 1.0 W m^{-2} (Table 2). Recalling that their analysis was done using monthly mean data, we compared our results obtained using monthly mean data with their values and found that our values are similar to theirs, although still about an order of magnitude smaller. The difference between G_e computed from daily and monthly data is mostly due to the radiative flux contributions becoming less negative. The sensible heat fluxes also become less negative, but not by as much as the radiative fluxes, and the latent heat flux does not change very much. This supports our belief that since G_e is related to phenomena such as storms, which vary on meteorological time scales, it is necessary to use daily data in order to resolve the zonal temperature and heating gradients properly.

To understand the role of clouds in the energy cycle, we repeated our computations of G_z and G_e using clear-sky radiative flux profiles from the ISCCP-FD dataset in order to determine how clouds affect the radiative contributions to G_z and G_e. The clear-sky radiative fluxes are computed by the GISS GCM radiation code using the same observed temperature and humidity profiles from TOVS used for the full-sky computations [minus some small adjustments, described in Zhang et al. (2004)], except without the clouds. Everything else is kept the same. Thus, the clear-sky values of G_z and G_e we obtained are not what would exist if there were no clouds, since in that case there would be no precipitation and very different atmospheric and surface conditions.

Table 2 presents the column totals for the clear-sky case, as well as the percent change from the full-sky values. The value of G_z is more strongly affected than G_e, with reductions of anywhere from about 50% to more than 150%. The magnitude of the differences between clear-and full-sky G reveals the importance of cloud radiative effects on the circulation and suggests that prior estimates of G may also have suffered from incomplete global coverage of clouds. In the NH, the

TABLE 2. Estimates of the generation of available potential energy (W m^{-2}) for the NH, SH, and global atmosphere [after Peixoto and Oort (1992)] computed using clear-sky radiation and the percent change from the values computed using full-sky radiation. As in Peixoto and Oort, to obtain the integrals over the total atmospheric mass, multiply the values for the NH and SH by 2.56×10^{14} m^2 and the values for the globe by 5.12×10^{14} m^2.

		Year			DJF			MAM			JJA			SON		
		NH	SH	Globe	NH	SH	Globe	NH	SH	Globe	NH	SH	Globe	NH	SH	Globe
G_z	Column tot	0.33	0.41	0.37	0.24	−0.10	0.07	−0.38	0.77	0.20	0.46	0.94	0.70	1.04	−0.01	0.52
	Change (%)	−76	−75	−76	−84	−110	−94	−160	−65	−86	−64	−59	−61	−52	−101	−68
G_e	Column tot	−0.34	−0.33	−0.34	−0.32	−0.23	−0.27	−0.43	−0.37	−0.40	−0.24	−0.39	−0.32	−0.38	−0.32	−0.35
	Change (%)	−13	−22	−17	−52	−21	−35	−13	−28	−18	−14	−22	−19	−12	−23	−17

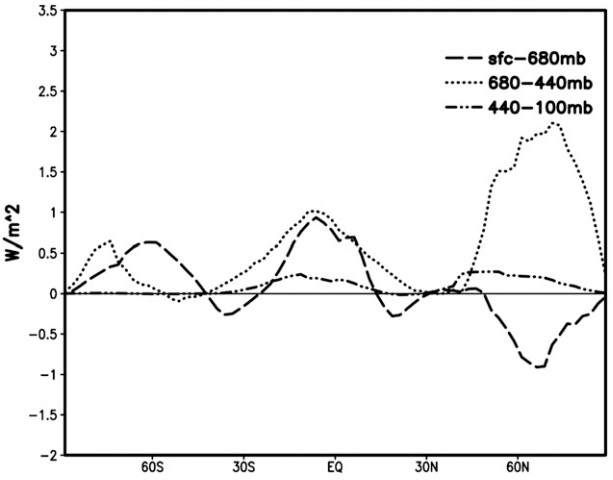

FIG. 13. Difference between DJF mean full- and clear-sky contributions from each latitude to global G_z. Values are computed from daily mean, temperature, and diabatic heating and have been weighted by the cosine of latitude.

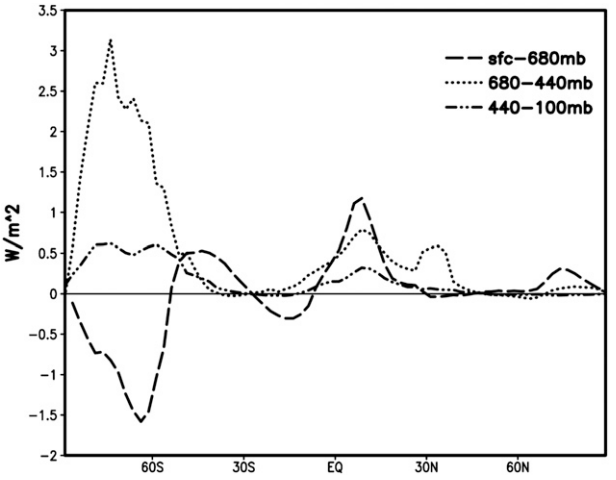

FIG. 14. As in Fig. 13, but for JJA.

largest reductions in G_z are in DJF and MAM, whereas the largest reductions in the SH are in DJF and SON. In some cases, G_z changes sign from positive to negative; G_e is also affected by the loss of clouds, but not by as much as G_z. Clear-sky G_e values become even more negative, by around 10% to as much as about 50%, with the largest magnitude change in the NH winter and smallest in the NH summer. SH reductions (i.e., larger negative values of G_e) are more consistent from season to season, generally about 25%. The value of G_e is always negative in the hemispheric and global mean, and it becomes more so without cloud radiative effects, especially in the NH winter.

Figures 13 and 14 show the difference between full-sky and clear-sky G_z as a function of latitude and height for DJF and JJA. They demonstrate that clear-sky G_z is considerably smaller than full-sky G_z, especially in the tropics and winter mid-to-high latitudes. Clouds decrease radiative cooling in the tropics throughout the troposphere, but most strongly in the lower and middle troposphere, and so act to reduce the latitudinal gradient of radiative cooling. Because radiation is negatively correlated with temperature, reducing the latitudinal temperature gradient increases G_z. At the poles, clouds warm the lower troposphere but cool the middle and upper troposphere during winter. The strong cooling at the poles, especially in combination with the tropical heating caused by clouds, reverses the sign of the latitudinal radiative flux gradient in the middle and upper troposphere from neutral or slightly anticorrelated with temperature to positively correlated with temperature (not shown).

In general, removing clouds has little effect on zonal mean G_e, except in the NH winter midlatitudes. Figure 15 shows that clouds enhance G_e production at low and middle levels of the troposphere in the storm tracks of the winter hemisphere. Clouds mitigate the tendency of radiation to damp the eddy temperature structure, especially in the midlatitude storm tracks, where the clouds act to warm the warm sector of a baroclinic wave, while the absence of clouds in the cold sector allows rapid radiative cooling.

Our investigation of the spatial distribution of G_z and G_e and the contributions to them from the individual diabatic heating terms permits us to form a picture of which processes are important to the generation of available potential energy and where. Latent heating from convection and radiative flux convergence associated with upper-level clouds and water vapor in the ITCZ contribute to the production of G_z in the tropics of the summer hemisphere. Contributions to G_z from surface sensible heat flux are reduced in the summer

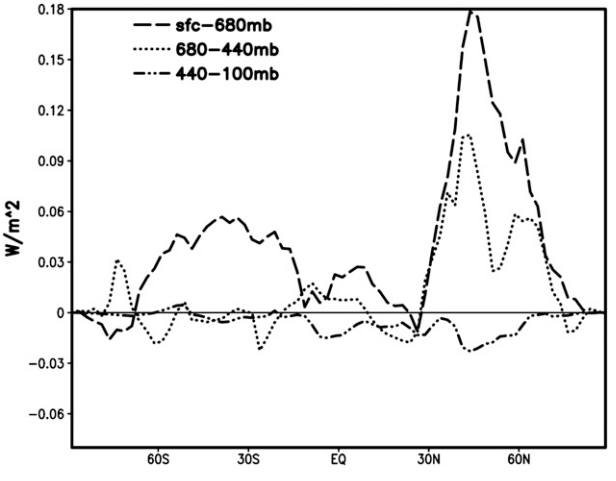

FIG. 15. As in Fig. 13, but for G_e.

tropics because cloud cover inhibits heating of the surface but are enhanced in the tropics of the winter hemisphere as subsidence inhibits cloud formation, permitting more sunlight to heat the surface, while contributions from latent heating and radiative flux are smaller in the winter tropics. An interplay between radiative and surface flux contributions to G_z also exists in the poles during winter. Clouds increase the emissivity of the polar atmosphere, allowing larger radiative cooling than in clear-sky conditions, which increases G_z. At the same time, clouds prevent the surface from cooling via radiation, which decreases the temperature gradient between the surface and the atmosphere, thus reducing surface sensible heat flux to the surface from the atmosphere, which decreases the contribution to G_z from surface sensible heat fluxes. In clear conditions when the polar atmosphere's low emissivity prevents efficient radiative cooling to space, the surface is able to cool faster than the atmosphere (Stramler et al. 2011). This produces a large temperature difference between the atmosphere and surface that causes sensible heating of the surface by the atmosphere. In both the tropics and the poles, the presence or absence of clouds determines whether G_z is produced via radiative flux or surface sensible heat flux.

The quantity G_e can be thought of as having a negative background state caused by radiative damping of the eddy temperature structure. Clouds mitigate this tendency, thus acting to enhance G_e, and through it, the eddy circulation. The clouds that have the largest positive effect on G_e are those where baroclinic eddies organize the temperature and cloud fields so that the clouds warm the warm areas and the lack of clouds allows rapid radiative cooling of the cool areas. The resulting increase in G_e then provides additional energy for conversion, completing a feedback loop.

Production of G_e is higher in areas where there are quasi-stationary elements of the circulation that organize heating and temperature fields so as to maintain a positive correlation, such as the midlatitude storm tracks in winter and the Indian monsoon in summer (Figs. 5, 6). These elements depend on features found in the NH that have no analogs in the SH, such as the Himalayan plateau, and the distribution of continents and ocean in mid and high latitudes, which creates preferred cyclogenesis regions (planetary standing waves) and a strong zonal temperature contrast. Where the conditions are right for persistent circulation patterns to form, as in the NH, the dynamics tend to organize the clouds and precipitation so as to increase G_e.

In a dry atmosphere, the large-scale dynamics would tend to destroy the equator-to-pole temperature gradient, converting potential to kinetic energy and bringing the atmosphere closer to the reference state. However, cloud processes that are associated with the large-scale dynamics impede the relaxation toward the reference state, enhancing G_z and, thus, the zonal mean circulation via cloud processes: decreased radiative cooling (i.e., a relative warming) and increased latent heating of the rising branch of the ITCZ. This is a direct relationship between the zonal mean circulation and its thermal forcing, a positive feedback mediated by cloud processes, as has been previously noted (e.g., Raymond 2000; Sohn 1999; Rossow and Zhang 1995; Siegmund 1993; Sohn and Smith 1992a,b; Stuhlmann and Smith 1988a,b). It is tempting to make a similar argument for the poles, that the mean meridional circulation produces low pressure and, thus, net upward motion, favoring cloud formation, which enhances G_z production, thereby increasing the forcing for the mean meridional circulation. However, this view of polar dynamics is contradicted at least in the Northern Hemisphere by recent work showing the existence of two atmospheric modes in the northern polar winter: a cold, clear-sky mode where the surface cools to space and a warm, cloudy mode where the atmosphere cools to space (Stramler et al. 2011). In this view, the connection between the zonal mean circulation and enhanced G_z production via clouds is less direct, as it is the eddy circulation, rather than the zonal mean circulation, that determines whether the cold or warm mode is present at any given time and thus determines whether G_z is produced via radiative or surface sensible heat fluxes.

6. Conclusions

The quantities G_z and G_e were computed directly from daily mean global temperature and diabatic heating fields for 1997–2000. The global annual mean G_z is 1.52 W m^{-2}. Values reach a minimum of 0.63 W m^{-2} in the NH during spring and a maximum of 2.27 W m^{-2} during SH winter. The largest contributors to G_z are latent heating in the tropical upper troposphere associated with the ITCZ in the summer hemisphere and surface sensible heat fluxes in the winter pole, while radiative fluxes generally destroy G_z via longwave cooling. However, clouds act to reduce the radiative destruction of G_z; in other words, the clouds produced by the atmospheric circulation cause a positive radiative feedback.

The quantity G_e is negative and about an order of magnitude smaller than G_z, with a global annual mean of -0.29 W m^{-2}. The small value of G_e results from the cancellation of the contributions from the individual diabatic heating terms. Contributions from latent heating and radiative fluxes are of comparable size to their

contributions to G_z, while contributions from surface sensible heat fluxes are smaller. The cancellation is not spatially homogeneous, so there are regions of large G_e production and destruction, suggesting that although the contributions from the three diabatic heating terms tend to cancel each other in the global mean, they enhance or suppress the circulation on a more regional scale, especially in the NH. Latent heating is a positive contributor, while radiative fluxes remove G_e. The latter effect is, however, mitigated by cloud perturbations of radiation. Surface sensible heat fluxes also remove G_e, in contrast to their role in G_z production, where they are strong contributors. This is in agreement with Lorenz's (1955) supposition that G_e would be negative because of radiational damping of the eddy temperature field, but that this would be partly offset by the tendency of latent heating to occur in warmer longitudes. In NH winter, the midlatitude storm tracks are important regions of G_e production, while the subtropical deserts and the Indian monsoon dominate in NH summer.

Access to globally complete measurements of temperature and diabatic heating has permitted us to identify how each type of heating contributes to G_z and G_e and the spatial distribution of the individual contributions. We are able to use the information to try to diagnose which processes are responsible for generating available potential energy in different locations on the globe. For instance, we found that latent heating is important to G_z in the tropics, especially at mid to high levels in the summer hemisphere. We can then infer that deep convection associated with the ITCZ generates available potential energy, confirming earlier statements to that effect (Stuhlmann and Smith 1988a,b). We learned that surface sensible heat fluxes are a large contributor to both G_z and G_e, particularly in the mid and higher latitudes, but act in opposite ways. This indicates the importance of interactions between the surface and the atmosphere to both large- and small-scale circulation patterns, even though the fluxes are relatively small.

Radiation's effectiveness in removing G_z and G_e is strongly mitigated by clouds. In the summer hemisphere tropics, clouds associated with the ITCZ greatly inhibit radiative cooling, whereas in the winter poles, clouds increase the atmosphere's opacity and permit more efficient cooling, both effects acting to enhance G_z production compared to the clear-sky case. In both the tropics and the poles, cloud effects on surface insolation inhibit G_z production by surface sensible heat fluxes (heat transfer from the surface to the atmosphere in the case of the warm, sunny tropics and heat transfer from the atmosphere to the surface in the case of the cold, dark winter pole). Since longwave radiative fluxes vary more strongly with temperature than surface sensible heat fluxes, clouds on the whole enhance G_z, as the reduction in the destruction of G_z by radiation outweighs the loss of the contribution to G_z from surface sensible heat fluxes. Similarly, clouds inhibit production of G_e by surface sensible heat fluxes over land by reducing shortwave absorption by the surface and subsequent sensible heat transfer to the atmosphere in summer and sensible heat transfer to the surface from the atmosphere in winter. Clouds do not mediate the surface–atmosphere interaction over the ocean as much, but they still reduce radiative damping of the eddy temperature structure. Cloud influences on G_e are largest in locations where quasi-stationary circulation features exist, such as the NH winter midlatitude storm tracks and the Indian monsoon.

Because temperature gradients are largest near the surface, surface sensible heat fluxes strongly affect both G_z and G_e, despite their small magnitude compared to latent and radiative fluxes. Surface sensible heat fluxes are always positive contributors to G_z and are especially effective in the winter hemisphere as radiative cooling of the polar surface leads to the subsequent transfer of sensible heat from the atmosphere to the surface, enhancing the covariance of the latitudinal gradients of sensible heat flux and temperature and thus producing G_z. With the exception of the NH summer, where sensible heating over the hot, dry deserts of the Sahara and the Middle East enhances the covariance between temperature and surface sensible heat flux, surface sensible heat fluxes behave the opposite with respect to G_e; that is, they destroy G_e rather than create it. Destruction of G_e by surface sensible heat fluxes is especially pronounced in the NH winter at the eastern coasts of Europe and Asia and over western Europe. These patterns are nearly nonexistent in the corresponding SH seasons, suggesting that the configuration of ocean and continents is important in determining the contribution of surface sensible heat fluxes to G_e.

The results presented herein suggest that the large-scale dynamics of the atmosphere organize the spatial and temporal distribution of clouds and precipitation in such a way as to increase the energy available to the circulation. Of course, it is important to keep in mind that the diabatic heating terms and the temperature are not independent of one another or of the circulation: each feeds back on the others on various space and time scales, so that each component is always responding to changes in the other components and then inducing further changes, and so on.

Acknowledgments. This work was supported by the National Aeronautics and Space Administration Modeling,

Analysis, and Prediction Program under Don Anderson (NASA Grant NNXD7AN04G) and by the National Aeronautics and Space Administration Energy and Water Cycle Study project under Jared Entin (NASA Grant NNXD7AO90G). The authors wish to thank Tony Del Genio, Adam Sobel, Lorenzo Polvani, and Johnny Luo, as well as several anonymous reviewers, for their helpful comments and suggestions.

APPENDIX

Sensitivity Analyses

Table A1 summarizes the results of our sensitivity studies, which are described briefly below. On the basis of estimates of the annual mean global atmospheric water cycle (evaporation–precipitation, which should balance in the long-term mean), the precipitation dataset we used (GPCP) is thought to underestimate total global precipitation by 5% in the long-term average but up to 10% in any given year (Schlosser and Houser 2007). Studies currently underway suggest a somewhat lower bias than 10% is probable, even at high latitudes (Bolvin et al. 2009), where the uncertainty is largest (Adler et al. 2003). We considered three scenarios: one in which an underestimate is due solely to underestimating precipitation from 60° to 90°N (resulting in an error in both the magnitude of the precipitation and its latitudinal gradient), one in which precipitation is underestimated from 60° to 90°S, and one in which the latitudinal gradient is correct but precipitation all over the globe is underestimated equally. For the latitudinal gradient tests, we altered the precipitation values at every location between 60° and 90°N(S), such that the zonal mean precipitation for that region is equal to the zonal mean precipitation from 50° to 60°N(S), effectively greatly reducing the latitudinal gradient. This produced an increase in global total precipitation of about 5%–15% day^{-1}. For the magnitude only test, we added enough precipitation to every location on the globe to increase the global total by 15%. The amount of precipitation added was about 0.35 mm day^{-1} per grid box.

Since it is unlikely that the precipitation underestimate is confined solely to a single polar region, the uncertainty of G_z lies somewhere between the results of our three test cases. The results suggest that our G_z could be too large during NH winter and SH winter and summer (Table A1, tests 1a–c) because of errors in the latitudinal gradient of precipitation.

Our profiles of latent heating peak in the upper troposphere in the tropics and in the summer midlatitudes and in the midtroposphere otherwise. The 3-yr (1997–99) tropical mean latent heating profiles derived from TRMM data presented in Fig. 6 of Tao et al. (2006) show peak heating between 6 and 8 km, or roughly 350–450 mb. Our upper tropospheric layer extends from 440 to 100 mb, so it is possible that our scheme places the peak heating higher than it should be. We constructed a test dataset in which the altitude of peak heating in the tropics (30°N–30°S) is moved downward by multiplying the values in the midtroposphere by 2 and the upper troposphere by 0.5 and then normalizing to preserve the original column total heating. Profiles at mid and high latitudes are not changed.

Our results show that our G_z may be too small, especially in the SH summer, because of errors in the vertical partitioning of latent heating (Table A1, test 2). The ISCCP TOVS near-surface temperatures are thought to be too warm in the polar regions during winter because they do not adequately capture the persistent surface inversions (Zhang et al. 2006). We tested the sensitivity of our results to this possible source of error by subtracting 4 K from DJF temperatures from 70° to 90°N, 3 K from 66° to 69°N, 2 K from 63° to 65°N, and 1 K from 60° to 62°N in the lower troposphere layer. We found negligible sensitivity to this error (Table A1, test 3).

The possible error in polar winter temperatures implies that the radiative fluxes from the lower troposphere may be too large. We tested the sensitivity of our results to this error by lowering the magnitude of the lower troposphere cooling from 70° to 90°N during DJF by 15 W m^{-2} and then smoothing the zonal radiative flux profile from 60° to 70°N to avoid spurious sharp latitudinal gradients. Our results show that this error in high-latitude radiative fluxes has negligible effects except in NH winter, when our estimate of G_z could be too large (Table A1, test 4).

The smallest radiative cooling occurs in the upper troposphere in our dataset, with larger cooling in both the mid and lower troposphere. Other studies show more consistent cooling throughout the column: see, for example, Sheu and Curry (1992) for radiative heating profiles over the North Atlantic and McFarlane et al. (2007) for profiles over Nauru and Manus in the tropical Pacific. To test sensitivity to the shape of the radiative heating profile in the tropics while preserving the column total radiative heating, we reduced the gradient between the lower and middle troposphere by 50% by increasing cooling in the midtroposphere and decreasing cooling in the lower troposphere by 25% of the difference between the two between 30°N and 30°S in all seasons. We found that the effect of the radiative heating vertical gradient was generally small, but it could produce too large values of G_z in SH summer (Table A1, test 5).

To explicitly test the sensitivity of G_e to a zonally varying data error, we created a test dataset with a land–ocean bias

TABLE A1. Results of sensitivity studies. Up (down) arrows denote an increase (decrease) in G computed using the data altered for that particular sensitivity study. Values in parentheses refer to the effect of the sensitivity study on G_e.

Test	Effect on G_z (G_e)				Implications
	NH JJA	SH DJF	NH DJF	SH JJA	
1a. Precipitation bias (globally uniform)	↓4% (↓5%)	↓10% (↓5%)	↓5% (↓10%)	↓2% (↓6%)	Vertical apportioning changes gradients at different levels; effect on G is generally small. Unrealistic scenario, but could be overestimating G_z and G_e by a small amount.
1b. Precipitation latitude bias (northern polar)	↓29% (↓5%)	↓6% (no change)	↓77% (↓10%)	↑4% (↓3%)	Unrealistic scenario, but suggests NH G_z could be too high, especially in winter.
1c. Precipitation latitude bias (southern polar)	↓10% (↓5%)	↓104% (↓11%)	↑5% (↓5%)	↓69% (↓3%)	Unrealistic scenario, but suggests SH G_z could be too high in both summer and winter.
2. Precipitation vertical bias (tropics)	↑53% (↑5%)	↑94% (↑16%)	↑40% (no change)	↑20% (↓3%)	Unrealistic scenario, but suggests G_z could be too low, especially in SH summer.
3. Polar winter surface temp latitude bias	–	no change (no change)	↑5% (no change)	–	Negligible effect on both G_z and G_e.
4. Polar winter surface radiation latitude bias	–	↓2% (no change)	↓21% (no change)	–	Suggests NH winter G_z could be too high, negligible effect otherwise.
5. Radiation vertical bias (tropics)	↓4% (↑5%)	↓9% (no change)	↓7% (↑5%)	↓7% (↑3%)	Effect is generally small, could be overestimating G_z by a small amount in SH summer.
6. Land–water sensible heat contrast bias	↓2% (↑5%)	↓1% (↓11%)	↓11% (↓29%)	↑3% (↓6%)	Generally small effect, but could be overestimating G_z in NH winter and G_e in SH summer and NH winter.
Overall effect (linear sum of studies 2–6, plus the average of 1a, 1b, and 1c)	↑4% (no change)	↓38% (↓11%)	↓71% (↓49%)	↓51% (↓18%)	Test scenarios used more extreme biases than we believe to be present, especially scenarios 1a–c, 2, and 5. Given that, we believe that G_z is likely to be too high in NH winter and, by a lesser amount, in both SH winter and summer; G_e is probably not negative enough, especially in the NH winter.

in surface sensible heat flux by increasing the flux from land by 10 W m^{-2} everywhere in all seasons. We found the effects were generally small, with the largest influence on the NH winter G_e where the land–ocean contrast is most important (Table A1, test 6).

Additionally, G_z and G_e depend on global mean temperature and lapse rate through the stability term Γ. Uncertainty in the global mean lapse rate is on the order of 10% near the surface and smaller aloft (Zhang et al. 2004). Uncertainties in global mean temperature are even smaller, on the order of a few Kelvins, or 1% of the global mean temperature. As seen in Eqs. (1) and (2), errors of this magnitude in global mean temperature and lapse rate, even if present over the entire globe, will only change G_z and G_e by a tiny constant.

Overall, the sensitivity test results summarized in Table A1 suggest that we may have overestimated G_z by as much as 20% during SH summer, 25% during SH winter, and 35% during NH winter. We may have underestimated the magnitude of G_e (a negative value, i.e.,

our value is probably not negative enough) by as much as 25% during NH winter, 10% during SH winter, and by a lesser amount otherwise.

REFERENCES

Adler, R. F., and Coauthors, 2003: The version-2 Global Precipitation Climatology Project (GPCP) monthly precipitation analysis (1979–present). *J. Hydrometeor.,* **4,** 1147–1167.

Arpe, K., C. Brankovic, E. Oriol, and P. Speth, 1986: Variability in time and space of energetics from a long series of atmospheric data produced by ECMWF. *Beitr. Phys. Atmos.,* **59,** 321–355.

Baldi, M., G. A. Dalu, and R. A. Pielke, 2008: Vertical velocities and available potential energy generated by landscape variability—Theory. *J. Appl. Meteor. Climatol.,* **47,** 397–410.

Boer, G., and S. Lambert, 2008: The energy cycle in atmospheric models. *Climate Dyn.,* **30,** 371–390, doi:10.1007/s00382-007-0303-4.

Bolvin, D. T., R. F. Adler, G. J. Huffman, E. J. Nelkin, and J. P. Poutiainen, 2009: Comparison of GPCP monthly and daily precipitation estimates with high-latitude gauge observations. *J. Appl. Meteor. Climatol.,* **48,** 1843–1857.

Brown, J. A., 1964: A diagnostic study of tropospheric diabatic heating and the generation of available potential energy. *Tellus,* **16,** 371–388.

Chen, T., W. B. Rossow, and Y.-C. Zhang, 2000: Radiative effects of cloud-type variations. *J. Climate,* **13,** 264–286.

Chou, S.-H., E. Nelkin, J. Ardizzone, R. M. Atlas, and C.-L. Shie, 2003: Surface turbulent heat and momentum fluxes over global oceans based on the Goddard satellite retrievals, version 2 (GSSTF2). *J. Climate,* **16,** 3256–3273.

Clapp, P. F., 1961: Normal heat sources and sinks in the lower troposphere in winter. *Mon. Wea. Rev.,* **89,** 147–162.

Curry, J. A., C. A. Clayson, W. B. Rossow, R. Reeder, Y. C. Zhang, P. J. Webster, G. Liu, and R. S. Sheu, 1999: High-resolution satellite-derived dataset of the surface fluxes of heat, freshwater, and momentum for the TOGA COARE IOP. *Bull. Amer. Meteor. Soc.,* **80,** 2059–2080.

——, and Coauthors, 2004: SEAFLUX. *Bull. Amer. Meteor. Soc.,* **85,** 409–424.

Curtis, S., R. Adler, G. Huffman, E. Nelkin, and D. Bolvin, 2001: Evolution of tropical and extratropical precipitation anomalies during the 1997–1998 ENSO cycle. *Int. J. Climatol.,* **21,** 961–971.

Dutton, J. A., and D. R. Johnson, 1967: The theory of available potential energy and a variational approach to atmospheric energetics. *Advances in Geophysics,* Vol. 12, Academic Press, 333–436.

Fuelberg, H. E., M. G. Ruminski, and D. O'C. Starr, 1985: Mesoscale generation of available potential energy in the warm sector of an extratropical cyclone. *Mon. Wea. Rev.,* **113,** 1150–1165.

Haimberger, L., and M. Hantel, 2000: Implementing convection into Lorenz's global cycle. Part II. A new estimate of the conversion rate into kinetic energy. *Tellus,* **52,** 75–92.

Hansen, A. R., and R. L. Nagle, 1984: Estimates of the generation of available potential energy by infrared radiation. *Mon. Wea. Rev.,* **112,** 1370–1377.

Hantel, M., and L. Haimberger, 2000: Implementing convection into Lorenz's global cycle. Part I. Gridscale averaging of the energy equations. *Tellus,* **52,** 66–74.

Hayashi, Y., and D. G. Golder, 1981: The effects of condensational heating on midlatitude transient waves in their mature stage: Control experiments with a GFDL general circulation model. *J. Atmos. Sci.,* **38,** 2532–2539.

Huffman, G. J., R. F. Adler, M. M. Morrissey, D. T. Bolvin, S. Curtis, R. Joyce, B. McGavock, and J. Susskind, 2001: Global precipitation at one-degree daily resolution from multisatellite observations. *J. Hydrometeor.,* **2,** 36–50.

Kalnay, E., and Coauthors, 1996: The NCEP/NCAR 40-Year Reanalysis Project. *Bull. Amer. Meteor. Soc.,* **77,** 437–471.

Kidwell, K. B., 1995: NOAA polar orbiter data user's guide. NOAA/NESDIS Guide, 394 pp.

Li, L., A. P. Ingersoll, X. Jiang, D. Feldman, and Y. L. Yung, 2007: Lorenz energy cycle of the global atmosphere based on reanalysis datasets. *Geophys. Res. Lett.,* **34,** L16813, doi:10.1029/2007GL029985.

Lin, B., and W. B. Rossow, 1997: Precipitation water path and rainfall rate estimates over oceans using special sensor microwave imager and International Satellite Cloud Climatology Project data. *J. Geophys. Res.,* **102,** 9359–9374.

Liu, Q., Y. F. Fu, R. C. Yu, L. Sun, and N. M. Lu, 2008: A new satellite-based census of precipitating and nonprecipitating clouds over the tropics and subtropics. *Geophys. Res. Lett.,* **35,** L07816, doi:10.1029/2008GL033208.

Lorenz, E. N., 1955: Available potential energy and the maintenance of the general circulation. *Tellus,* **7,** 157–167.

——, 1967: The nature and theory of the general circulation of the atmosphere. WMO-218 TP 115, 161 pp.

Magagi, R., and A. P. Barros, 2004: Estimation of latent heating of rainfall during the onset of the Indian monsoon using TRMM PR and radiosonde data. *J. Appl. Meteor.,* **43,** 328–349.

Marques, C. A. F., A. Rocha, J. Corte-Real, J. M. Castanheira, J. Ferreira, and P. Melo-Gonçalves, 2009: Global atmospheric energetics from NCEP–Reanalysis 2 and ECMWF–ERA40 Reanalysis. *Int. J. Climatol.,* **29,** 159–174.

McFarlane, S. A., J. H. Mather, and T. P. Ackerman, 2007: Analysis of tropical radiative heating profiles: A comparison of models and observations. *J. Geophys. Res.,* **112,** D14218, doi:10.1029/2006JD008290.

Oort, A. H., and J. P. Peixoto, 1976: On the variability of the atmospheric energy cycle within a 5-year period. *J. Geophys. Res.,* **81,** 3643–3659.

——, and ——, 1983: Global angular momentum and energy balance requirements from observations. *Advances in Geophysics,* Vol. 25, Academic Press, 355–490.

Pauley, P. M., and P. J. Smith, 1988: Direct and indirect effects of latent heat release on a synoptic-scale wave system. *Mon. Wea. Rev.,* **116,** 1209–1235.

Peixoto, J. P., and A. Oort, 1992: *Physics of Climate.* American Institute of Physics, 520 pp.

Raymond, D. J., 2000: The Hadley circulation as a radiative–convective instability. *J. Atmos. Sci.,* **57,** 1286–1297.

Robertson, F. R., and P. J. Smith, 1983: The impact of model moist processes on the energetics of extratropical cyclones. *Mon. Wea. Rev.,* **111,** 723–744.

Rodell, M., and Coauthors, 2004: The Global Land Data Assimilation System. *Bull. Amer. Meteor. Soc.,* **85,** 381–394.

Romanou, A., W. B. Rossow, and S.-H. Chou, 2006: Decorrelation scales of high-resolution turbulent fluxes at the ocean surface and a method to fill in gaps in satellite data products. *J. Climate,* **19,** 3378–3393.

Romanski, J., 2009: Investigating the role of diabatic heating in global atmospheric circulation and climate sensitivity: An energetics approach. Ph.D. thesis, Columbia University, 242 pp.

Rossow, W. B., and Y.-C. Zhang, 1995: Calculation of surface and top of atmosphere radiative fluxes from physical quantities based on ISCCP datasets: II. Validation and first results. *J. Geophys. Res.,* **100** (D1), 1167–1197.

——, A. W. Walker, D. E. Beuschel, and M. D. Roiter, 1996: International Satellite Cloud Climatology Project (ISCCP) documentation of new cloud datasets. World Meteorological Organization Rep. WMO/TD 737, 115 pp.

——, Y.-C. Zhang, and J. Wang, 2005: A statistical model of cloud vertical structure based on reconciling cloud layer amounts inferred from satellites and radiosonde humidity profiles. *J. Climate,* **18,** 3587–3605.

Schlosser, C. A., and P. R. Houser, 2007: Assessing a satellite-era perspective of the global water cycle. *J. Climate,* **20,** 1316–1338.

Sheu, R.-S., and J. A. Curry, 1992: Interactions between North Atlantic clouds and the large-scale environment. *Mon. Wea. Rev.,* **120,** 261–278.

Siegmund, P., 1993: Cloud diabatic forcing of the atmosphere, estimated from simultaneous ECMWF diabatic heating and ISCCP cloud amount observations. *J. Climate,* **6,** 2419–2433.

——, 1994: The generation of available potential energy: A comparison of results from a general circulation model with observations. *Climate Dyn.,* **11,** 129–140.

Smith, P. J., 1980: The energetics of extratropical cyclones. *Rev. Geophys.,* **18,** 378–386.

Sohn, B.-J., 1999: Cloud-induced infrared radiative heating and its implications for large-scale tropical circulations. *J. Atmos. Sci.,* **56,** 2657–2672.

——, and E. A. Smith, 1992a: The significance of cloud–radiative forcing to the general circulation on climate time scales—A satellite interpretation. *J. Atmos. Sci.,* **49,** 845–860.

——, and ——, 1992b: Global energy transports and the influence of clouds on transport requirements—A satellite analysis. *J. Climate,* **5,** 717–734.

Steinheimer, M., M. Hantel, and P. Bechtold, 2008: Convection in Lorenz's global energy cycle with the ECMWF model. *Tellus,* **60,** 1001–1022.

Stramler, K., A. D. Del Genio, and W. B. Rossow, 2011: Synoptically driven Arctic winter states. *J. Climate,* **24,** 1747–1762.

Stuhlmann, R., and G. L. Smith, 1988a: A study of cloud-generated radiative heating and its generation of available potential energy. Part I: Theoretical background. *J. Atmos. Sci.,* **45,** 3911–3927.

——, and ——, 1988b: A study of cloud-generated radiative heating and its generation of available potential energy. Part II: Results for a climatological zonal mean January. *J. Atmos. Sci.,* **45,** 3928–3943.

Suomi, V. E., and W. C. Shen, 1963: Horizontal variation of infrared cooling and the generation of eddy available potential energy. *J. Atmos. Sci.,* **20,** 62–65.

Tao, W.-K., and Coauthors, 2001: Retrieved vertical profiles of latent heat release using TRMM rainfall products for February 1988. *J. Appl. Meteor.,* **40,** 957–982.

——, and Coauthors, 2006: Retrieval of latent heating from TRMM measurements. *Bull. Amer. Meteor. Soc.,* **87,** 1555–1572.

Trenberth, K. E., and L. Smith, 2006: The vertical structure of temperature in the tropics: Different flavors of El Niño. *J. Climate,* **19,** 4956–4970.

——, J. M. Caron, and D. P. Stepaniak, 2001: The atmospheric energy budget and implications for surface fluxes and ocean heat transports. *Climate Dyn.,* **17,** 259–276.

——, D. P. Stepaniak, and J. M. Caron, 2002: Accuracy of atmospheric energy budgets from analyses. *J. Climate,* **15,** 3343–3360.

Turpeinen, O. M., L. Garand, R. Benoit, and M. Roch, 1990: Diabatic initialization of the Canadian Regional Finite-Element (RFE) model using satellite data. Part I: Methodology and application to a winter storm. *Mon. Wea. Rev.,* **118,** 1381–1395.

Zhang, Y.-C., W. B. Rossow, A. A. Lacis, V. Oinas, and M. I. Mischenko, 2004: Calculation of radiative flux profiles from the surface to top of atmosphere based on ISCPP and other global datasets: Refinements of the radiative transfer model and the input data. *J. Geophys. Res.,* **109,** D19105, doi:10.1029/2003JD004457.

——, ——, and P. W. Stackhouse Jr., 2006: Comparison of different global information sources used in surface radiative flux calculation: Radiative properties of the near-surface atmosphere. *J. Geophys. Res.,* **111,** D13106, doi:10.1029/2005JD006873.